ELSEVIER

International Journal of Mass Spectrometry 201 (2000) 109–120

International Journal of Mass Spectrometry

Spin–orbit induced predissociation dynamics of HCl^+ and HBr^+ ions: temporal and spectral representations

Mikhail V. Korolkov[a,*], Karl-Michael Weitzel[a,†], Sigrid D. Peyerimhoff[b]

[a] *Institut für Chemie, Physikalische und Theoretische Chemie, Freie Universität Berlin, Takustrasse 3, 14195 Berlin, Germany*
[b] *Institut für Physikalische und Theoretische Chemie, Universität Bonn, Wegeler Strasse 12, 53115 Bonn, Germany*

Received 8 October 1999; accepted 17 November 1999

Abstract

The spin–orbit induced predissociation dynamics of HCl^+ and HBr^+ ions have been investigated by numerical solution of four coupled time-dependent Schrödinger equations based on ab initio potential energy data. For HCl^+ exponential decay dominates for all vibrational levels in the electronic excited $^2\Sigma^+$ state. For HBr^+ pronounced nonexponential decay occurs due to significant multichannel competition. The comparison of temporal and spectral representations of the dynamics reveals that the derivation of dynamic information from experimental frequency domain spectra may be difficult in the case of multichannel competition. (Int J Mass Spectrom 201 (2000) 109–120) © 2000 Elsevier Science B.V.

Keywords: Predissociation dynamics; Predissociation spectra; Wavepacket analysis

1. Introduction

The spin–orbit induced predissociation is a special case of nonadiabatic processes whose importance in chemistry has recently been reviewed by Yarkony [1]. The trends induced by the spin–orbit interaction can be illustrated, e.g. by looking at a homologous series of compounds. Here, the hydrogen halide ions, HX^+ (X = F, Cl, Br, I), represent an interesting example. With increasing nuclear charge the spin–orbit effects increase accordingly. In this series the best studied cases are the spin–orbit induced predissociation of HCl^+ and HBr^+ ions. For both ions the ground state, $^2\Pi_i$ ($i = 1/2, 3/2$), and the first excited electronic state, $A\ ^2\Sigma^+$, are strongly bound. However, HX^+ ions can predissociate from higher vibrational levels of the $A\ ^2\Sigma^+$ electronic state by spin–orbit induced coupling to three repulsive electronic states of $^4\Sigma^-$, $^2\Sigma^-$, and $^4\Pi$ symmetry. For both, the HBr^+ and the HCl^+, this leads to X^+ fragments, i.e. Br^+ (^3P) + H, and Cl^+ (^3P) + H. In contrast, the direct dissociation of the $A\ ^2\Sigma^+$ states lead to different reaction channels, i.e. Br^+ (^1D) + H and Cl (^2P) + H^+, respectively.

The electronic states of the HBr^+ ion are well known from photoelectron spectra [2,3], fluorescence spectra [4–6], and predissociation spectra [7]. The potential energy curves relevant for the predissociation out of the $A\ ^2\Sigma^+$ state have also been studied by ab initio techniques [8]. A number of theoretical [8,9] and experimental data [2,7,10] are available on the

* korolkov@chemie.fu-berlin.de

Present address: B.I. Stepanov Institute of Physics, National Academy of Sciences of Belarus, Scarina Ave. 70, 220602 Minsk, Republic of Belarus.

† weitzel@chemi.fu-berlin.de

1387-3806/00/$20.00 © 2000 Elsevier Science B.V. All rights reserved
PII S1387-3806(00)00222-0

predissociation lifetime of HBr^+. Similar information is available for the electronic states of the HCl^+ ion from photoelectron spectra [11–13], fluorescence spectra [14,15], predissociation spectra [16], and from ab initio calculations [17,18].

Most of the available experimental and theoretical analyses of predissociation lifetimes assumed exponential decay of population by either applying the Fermi-Wentzel golden rule [19] approximation or by assuming a Lorentzian lineshape. However, pronounced nonexponential decay was observed in a recent study of the HBr^+ employing the numerical solution of coupled time-dependent Schrödinger equations [20]. In the HCl^+ ion the spin–orbit coupling is a factor of 5 smaller compared to the HBr^+ ion. This leads to differences in the characteristics of the predissociation dynamics, in particular significantly longer predissociation times. In the current work we extend our earlier analysis of the HBr^+ ion and compare its predissociation dynamics to that of the HCl^+ ion. Further, the aim of this work is to discuss the representation of the predissociation dynamics not only in the time but also in the frequency domain. The former should predict characteristic phenomena to be observed by femtosecond lasers, whereas the latter is expected to provide a convenient basis for comparison with frequency domain experiments employing nanosecond lasers.

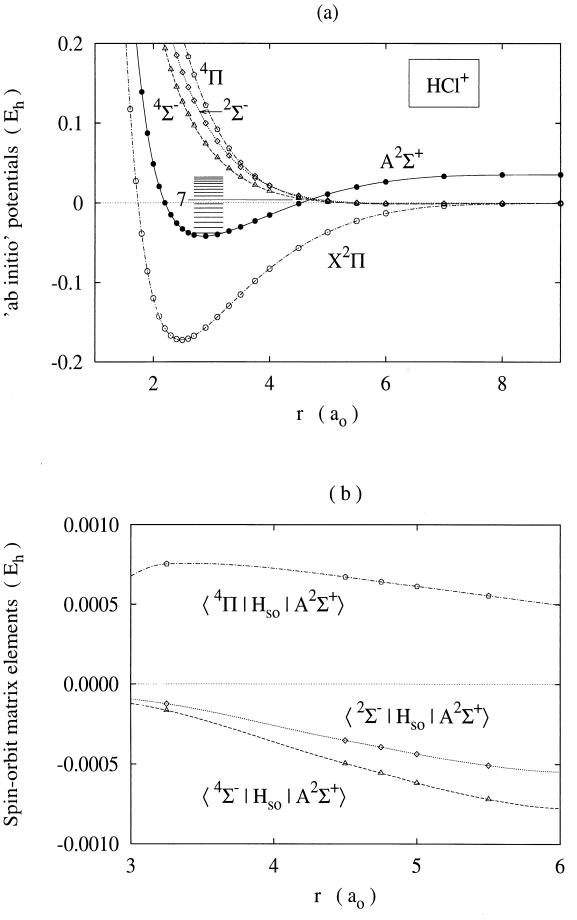

Fig. 1. (a) Potential energy curves of the HCl^+ ion relevant for the predissociation of the $A\ ^2\Sigma^+$ state. The curves have been obtained by cubic spline interpolation of data from [18] with modifications mentioned in the text. The vibrational eigenenergies calculated in this work are also indicated. (b) Spin–orbit matrix elements between the electronic states indicated.

2. Model and computational methods

In this work we employ the numerical solution of coupled time-dependent Schrödinger equations. Details of this approach have been presented elsewhere [20,21]. Only a brief description will be given here. Ab initio data for the HBr^+ potential curves were taken from Peyerimhoff and co-workers [8]. Ab initio data for the HCl^+ potential curves were taken from Dalgarno and co-workers [18]. For both systems the vibrational eigenenergies E_v and eigenfunctions $\chi_v(r)$ for the potential energy curve $V_A(r)$ have been calculated by the Fourier grid Hamiltonian method [22]. These vibrational eigenenergies are indicated in Figs. 1 and 2. In the case of HCl^+ the comparison of the vibrational eigenenergies with experimental frequencies [15,16] and, more important, the experimentally well known dissociation energy [23] yielded small but significant differences. Consequently the potential energy curve for the $A\ ^2\Sigma^+$ state of HCl^+ was scaled by about 2% in order to match the experimental data mentioned previously. A comparison of the vibrational eigenenergies of the HCl^+ is given in Table 1. The potential energy curves used in this work for HBr^+ and HCl^+ are presented in Figs. 1(a) and 2(a). In the case of HBr^+, a crossing between the bound

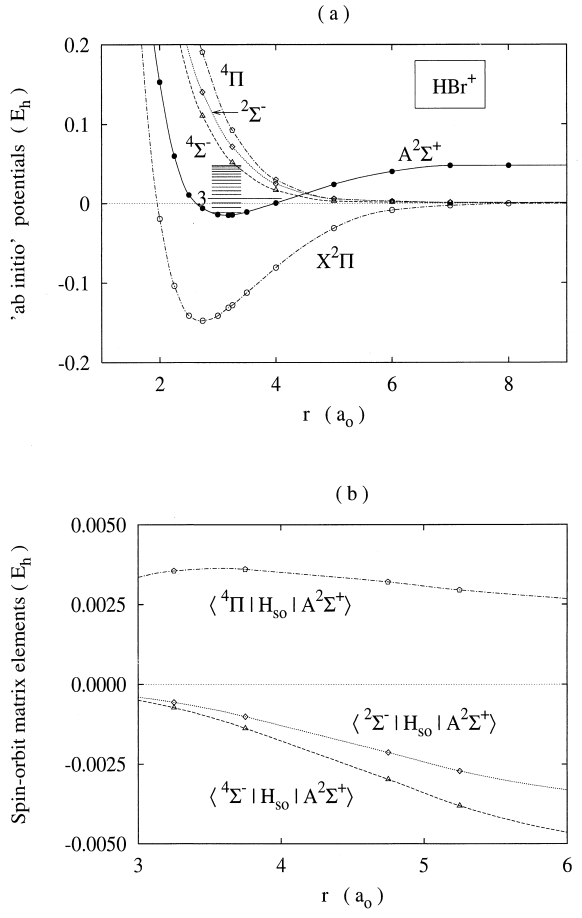

Fig. 2. (a) Potential energy curves of the HBr^+ ion relevant for the predissociation of the $A\ ^2\Sigma^+$ state. The curves have been obtained by cubic spline interpolation of data from [8]. The vibrational eigenenergies calculated in this work are also indicated. (b) Spin–orbit matrix elements between the electronic states indicated, data taken from [8].

and the repulsive states is observed in the region of v = 4. But the predissociation threshold occurs very close to the v = 2 vibrational state [7]. In HCl^+ on the other hand, the crossing occurs around v = 7, only slightly above the true predissociation threshold. We note that the slope of the repulsive states is considerably smaller for the HCl^+ compared to the HBr^+. This has an important impact on the predissociation dynamics.

The data for the relevant spin–orbit induced matrix elements,

$$H^{so}_{A,I}(r) = \langle \Psi^{el}(A\ ^2\Sigma^+)|\hat{H}_{so}|\Psi^{el}(^4\Sigma^-)\rangle_x$$

$$H^{so}_{A,II}(r) = \langle \Psi^{el}(A\ ^2\Sigma^+)|\hat{H}_{so}|\Psi^{el}(^2\Sigma^-)\rangle_x$$

$$H^{so}_{A,III}(r) = \langle \Psi^{el}(A\ ^2\Sigma^+)|\hat{H}_{so}|\Psi^{el}(^4\Pi)\rangle_x$$

are taken from ab initio calculations, Table 9 from [8] in the case of HBr^+, those for HCl^+ are given in Table 2. The latter have been obtained from multireference configuration interaction (MRD-CI) [24] calculations of the relevant electronic states with the spin–orbit operator in the Breit-Pauli form [25] in analogy to the HBr^+ calculations [8]. In this work the spin–orbit matrix elements for the spherical harmonic representation have been used. These matrix elements are also plotted in Figs. 1(b) and 2(b). The general trends are quite similar for the two molecular ions. However, the spin–orbit coupling strength is about a factor of 5 smaller in HCl^+ compared to HBr^+.

In the present work the quantum dynamics of the HX^+ molecular ions are described by four coupled time-dependent Schrödinger equations for the nuclear wave functions $\Psi_j(r, t)$ of the first bound excited (j = A) and the three repulsive (j = I, II, III) states:

$$i\hbar \frac{\partial \Psi_A(r, t)}{\partial t} = [\hat{T} + V_A]\Psi_A + \sum_{j=\mathrm{I}}^{\mathrm{III}} H^{so}_{A,j}(r)\Psi_j(r, t) \quad (1)$$

$$i\hbar \frac{\partial \Psi_j(r, t)}{\partial t} = [\hat{T} + V_j]\Psi_j + H^{so}_{A,j}(r)\Psi_A(r, t), \quad j = \mathrm{I, II, III} \quad (2)$$

where $\hat{T}$ is the kinetic-energy operator. The nuclear wave functions $\Psi_j(r, t)$ are represented on an equidistant N-point spatial grid in the coordinate space with first point r_{min} = 1.5 a_0, spatial step Δr = 0.02 a_0, and the last point from r_{max} = 83.4 a_0 to r_{max} = 656.84 a_0 for N = 4096 and N = 32768, respectively. Both, the split-operator method [26] and the integral equation method [21] are used for the propagation of the wave functions given in Eqs. (1) and (2) in time with time steps of $\Delta t \leq 1$ atomic unit (≈0.024 fs). The absorbing boundary [27] is used to prevent the artificial reflection of all $\Psi_j(r, t)$ wave functions at the edge of the grid.

Table 1
Comparison of the vibrational energies employed in this work for the HCl^+ with relevant data

Vibrational quantum no.	Energy (cm^{-1})[a]	Energy (cm^{-1})[b]	ΔE (col 2–col 3) (cm^{-1})	Energy (cm^{-1})[c]	ΔE (col 2–col 5) (cm^{-1})	Energy (cm^{-1})[d]
0	0	0	0	0	0	
1	1509	1500	8.8	1526	−16.8	
2	2946	2920	26.3	2975	−29.4	
3	4314	4267	47.8	4351	−36.8	
4	5612	5573	38.5	5654	−42.1	
5	6843	6815	27.5	6884	−41.4	
6	8007	7985	22.6	8041	−33.9	8010
7	9111	8985	126.5			
8	10147	9969	177.7			
9	11111	10905	206.0			
10	12008	11760	248.8			
11	12835	12631	204.6			
12	13591	13316	274.8			
13	14266	13961	304.3			
14	14853					
15	15349					

[a] This work.
[b] See [3].
[c] See [15].
[d] See [16].

The projection of the time-dependent wave function $\Psi_A(r, t)$ on the vibrational eigenstates $\chi_v(r)$, yields the time-dependent populations of the vibrational states

$$C_v(t) = |\langle\chi_v(r)|\Psi_A(r, t)\rangle|^2 . \quad (3)$$

The HBr^+ ion is assumed to be initially (i.e. at $t = 0$) in one of its eigenstates, without any populations of other states:

$$\Psi_A(r, t = 0) = \chi_v(r),$$
$$\Psi_j(r, t = 0) = 0, \qquad j = \text{I, II, III.} \quad (4)$$

In general predissociation cross sections can be obtained by calculating the square of the Fourier transform of the autocorrelation function [28]. In our case the autocorrelation function for the given initial conditions ($\langle\chi_v(t = 0)|\Psi(t)\rangle$) is complex. However, the square of the absolute value of this autocorrelation function corresponds to a real experimental observable, i.e. the population of the initial eigenstate [see Eq. (3)]. For comparison with experimental data it is also interesting to discuss the time dependence of the norm of the wave packet $\langle\Psi(t)|\Psi(t)\rangle^2$. The latter correlates directly with the number of product ions detected in a predissociation experiment [16]. Consequently Fourier transform spectra have been calculated by fast Fourier transformation (FFT) of the wave packet ($|\Psi_A(t)|^2$) of the excited electronic state and

Table 2
Spin–orbit coupling matrix elements in cm^{-1} for the complex spherical harmonic wave function for the relevant electronic states indicated

r (a.u.)	3.25	4.50	4.75	5.0	5.5
$\langle A\ ^2\Sigma^+\|\hat{H}_{so}\|^4\Sigma^-\rangle$	−36.3	−109.0	−122.1	−135.7	−157.8
$\langle A\ ^2\Sigma^+\|\hat{H}_{so}\|^2\Sigma^-\rangle$	−27.2	−77.5	−86.6	−96.0	−111.4
$\langle A\ ^2\Sigma^+\|\hat{H}_{so}\|^4\Pi\rangle$	165.4	147.3	140.8	134.6	121.8

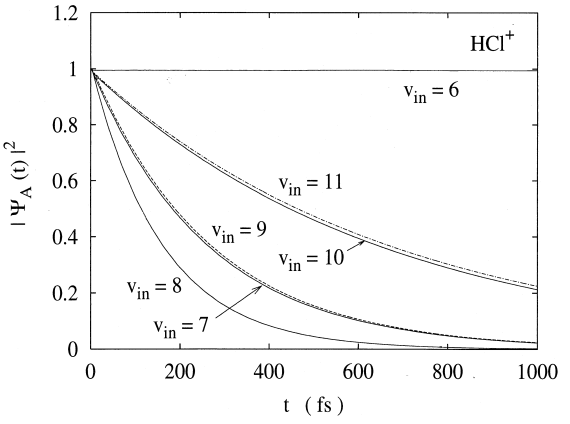

Fig. 3. Predissociation dynamics of HCl^+ ions in their $A\ ^2\Sigma^+$ electronic state: time evolution of $|\Psi_A(t)|^2$ for initial vibrational levels v = 6, 7, 8, 9, 10, and 11.

Table 3
Comparison of lifetimes derived in this work for the HCl^+ with data from the literature; for v = 11 the lifetimes calculated for the individual channels are given in parentheses

	Lifetime τ (1/e) (fs)		
Vibrational state with quantum number v	Wave packet dynamics	Golden rule[a]	Penno et al.[b]
6	20000		
7	262	8600	260
8	160	34	>46
9	266	61	
10	649	51	
11	672	240	
	(ch1: 949 ch2: 5295 ch3: 4068)		

[a] See [9].
[b] See [16].

the populations $C_i(t)$ of the vibrational eigenstates of this electronic state. For technical reasons the Fourier transformation was done from time to momentum (k) space. Since the energy E is proportional to k^2, we need to discuss the square of the Fourier transformation. Throughout this work the latter is referred to as a "spectrum."

3. Results

3.1. Vibrational predissociation dynamics of HCl^+ ions

The predissociation dynamics of HCl^+ ions initially prepared in the vibrational eigenstates v = 6–11 is shown in Fig. 3(a). $|\Psi_A(t)|^2$ is basically constant for level v = 6 in line with the fact that this level is below the threshold for predissociation. For all higher vibrational states decay is observed on the femtosecond time scale. From this data we can derive predissociation lifetimes (time for decay to 1/e). A comparison of the lifetimes of HCl^+ determined in this work with data available from the literature is presented in Table 3. Evidently the lifetime decreases from v = 6 to v = 8 and increases again for the higher vibrational states. The time evolution is clearly exponential for most of the initial vibrational levels. Accidentally the decay dynamics from the vibrational levels v = 7 and 9 and v = 10 and 11 are very similar. It is interesting to complement these dynamics in the time domain with the corresponding spectra in the frequency domain. These spectra can be calculated by Fourier transformation of the time-dependent wave packet. For a truly exponential decay in the time domain one would expect a perfect Lorentzian lineshape in the frequency domain. Fig. 4 shows the Fourier transform spectrum of the wave packet ($|\Psi_A(t)|^2$) for three different initial levels v = 7, 8,

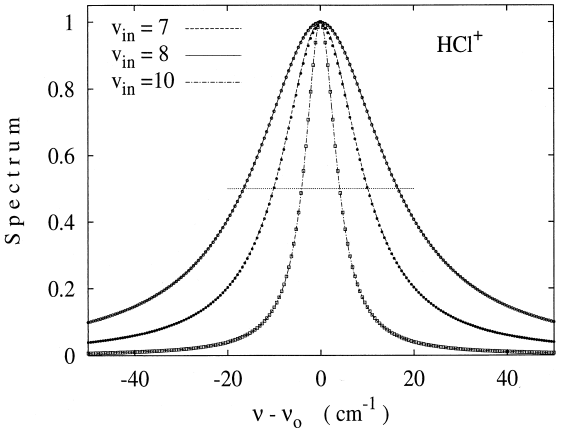

Fig. 4. Predissociation spectrum for the initial vibrational levels v = 7 (solid circles), 8 (open circles), and 9 (open squares). For each case a Lorentzian function is shown as a line.

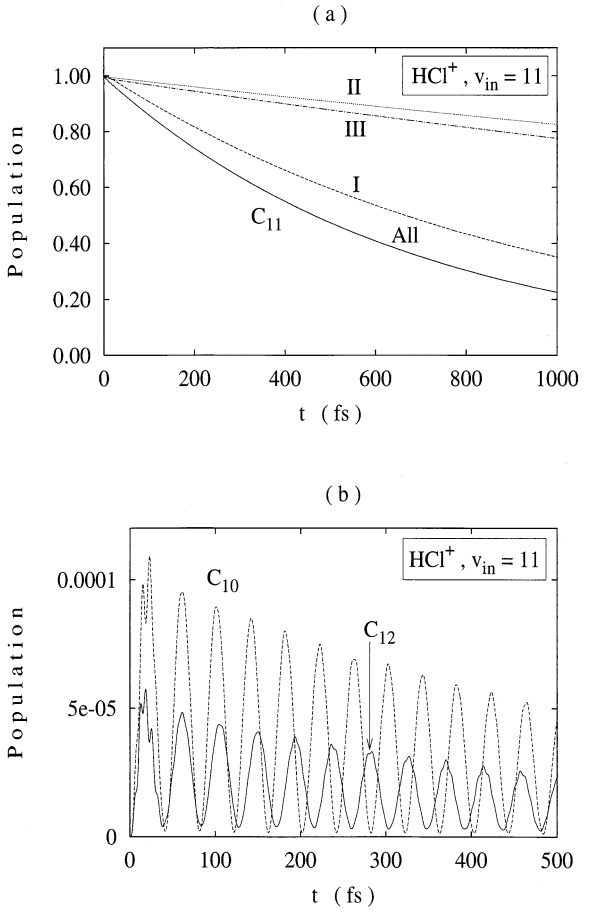

Fig. 5. Predissociation dynamics of HCl^+ from the initial level v = 11; (a) time evolution of $|\Psi_A(t)|^2$ and the population $C_{11}(t)$ (note, that the two are basically indistinguishable on the scale shown); $|\Psi_A(t)|^2$ obtained when taking into account only one of the three reaction channels (I, II, and III) separately are also shown. (b) Time evolution of the neighbouring levels $C_{10}(t)$ and $C_{12}(t)$.

and 10. For comparison we also show three Lorentzian functions with the appropriate full width at half maximum (FWHM). For v = 8 and v = 10 the Fourier transform of the wave packet appear to have an almost perfect Lorentzian lineshape. Only for $v = 7$ (solid circles) we note small but significant differences, particularly in the region of the center frequency.

Fig. 5 presents a more detailed analysis of the predissociation dynamics of HCl^+, v = 11. Fig. 5(a) presents the time evolution of $|\Psi_A(t)|^2$ including the interaction of the $^2\Sigma^+$ state with only one of the repulsive states (marked by the channel numbers I, II, and III) as well as $|\Psi_A(t)|^2$ including multichannel interaction between the predissociative state and all repulsive states (marked: All). The predissociation channel I (interaction with the $^4\Sigma^-$ state) clearly dominates. From this plot we derived lifetimes due to the interaction with the individual predissociation channels of 949 fs (I), 4.068 ps (III), and 5.295 ps (II). Assuming that the three channels are independent one would expect a total predissociation lifetime of 671.9 fs. The decay curve of $|\Psi_A(t)|^2$ including all channels simultaneously leads to a lifetime of 672.2 fs. This demonstrates that multichannel competitions are of no importance in this particular process and all channels operate independently. For comparison Fig. 5(a) also shows the decay of the population of the initial vibrational level v = 11, C_{11}. The lifetime for C_{11} is very similar to that for $|\Psi_A(t)|^2$, in fact the two decay curves are hardly distinguishable. However, the two neighbouring levels (v = 10 and 12) are excited and display pronounced oscillations [Fig. 5(b)]. The amplitude of these oscillations is indeed very small (<0.0001) and only weakly damped over the 500 fs time range shown. Some other neighbouring levels (9, 13, etc.) are also excited, but their amplitude is even smaller. The population of all these neighbouring levels builds up within the first 20 fs.

However, the oscillation frequency is smaller for C_{10} compared to C_{12}. At the time of formation C_{10} and C_{12} are in phase, around 280 fs the two are out of phase and at 500 fs they are again in phase. The difference in the recurrence frequency of C_{10} and C_{12} becomes even more clear when looking at the Fourier transform spectrum of these populations, shown in Fig. 6. The spectra of all three populations shown there (C_{10}, C_{11}, and C_{12}) exhibit a resonance at the central frequency ν_0. The width of this resonance correlates with the lifetime of the corresponding population. We note that this width is marginally smaller for C_{10} (7.83 cm^{-1}) than for C_{11} (7.92 cm^{-1}), but slightly larger for C_{12} (8.5 cm^{-1}). Only for the spectra of the populations C_{10} and C_{12} we observe side bands, but not for the spectrum of the population of the initial vibrational level v = 11. The actual

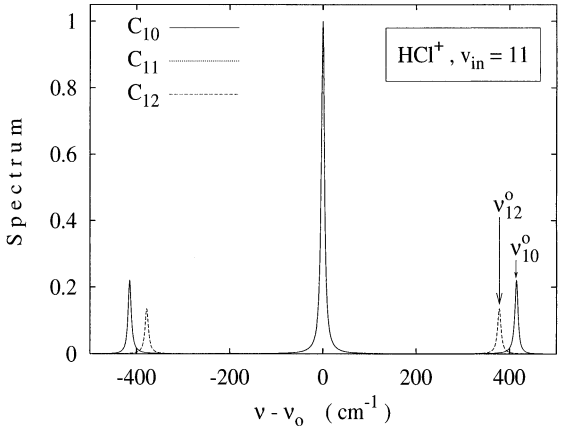

Fig. 6. Predissociation spectrum of the populations C_{10} (solid line), C_{11} (short dashed line), and C_{12} (long dashed line), initial vibrational level v = 11. Note that the sidewings are only observed for C_{10} and C_{12}. The relative position of unperturbed vibrational levels is marked by arrows.

position of these sidebands is $\nu^*_{10} = \pm 414.5$ cm^{-1} for C_{10} and $\nu^*_{12} = \pm 378.0$ cm^{-1} for C_{12}. very close to the resonance positions (826.8/2 = 413.4 and 755.8/2 = 377.9 cm^{-1}). Here, the factor of 2 arises from the fact that we present the Fourier transform of the population [see Eq. (3)] rather than that of the autocorrelation function itself.

The frequency difference between these two observed sidebands is 36.5 cm^{-1} as opposed to 35.5 cm^{-1} expected for the unperturbed vibrational levels. The difference is very small which is not surprising in the light of weak spin–orbit coupling. Because of this weak coupling the classical Landau-Zener picture would also give reasonable estimates of the energetic positions and splittings.

3.2. Vibrational predissociation dynamics of HBr^+ ions

In Sect. 3.1 we showed that the predissociation dynamics of the HCl^+ ion is basically exponential. We now turn our attention to the HBr^+ ion. Fig. 7 shows the time evolution of $|\Psi_A(t)|^2$ for HBr^+ ions initially prepared in the vibrational eigenstates v = 2 to v = 10 of the $^2\Sigma^+$ electronic state. The longest lifetime is observed for v = 2, which is the first

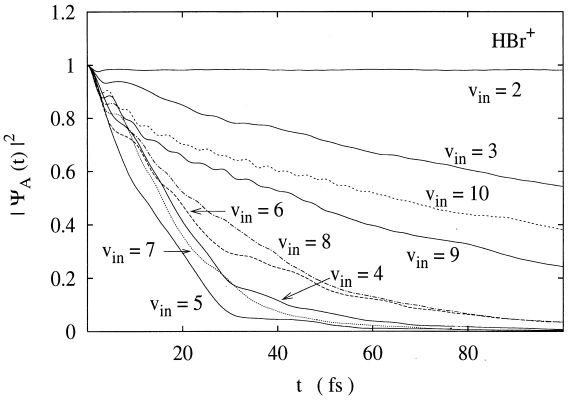

Fig. 7. Predissociation dynamics of HBr^+ ions in their $A\ ^2\Sigma^+$ electronic state; time evolution of $|\Psi_A(t)|^2$ for initial vibrational levels v = 2–10.

vibrational level above the predissociation threshold. The lifetime decreases from v = 2 to v = 5 before it increases again. Most of the decay functions shown are clearly nonexponential. The oscillations observed indicate significant redistribution of population within the first 50 fs. In the following we will concentrate on the temporal and spectral representation of the predissociation of HBr^+ ions initially prepared in the vibrational levels v = 5 and v = 9. More details regarding the predissociation dynamics of some other vibrational levels have been presented elsewhere [20].

Fig. 8 illustrates the predissociation dynamics of HBr^+ ions initially prepared in the v = 5 state. The time evolution of $|\Psi_A(t)|^2$ including all predissociation channels (All) and that taking into account only one channel at a time (marked I, II, and III) are shown in Fig. 8(a). For most of the time predissociation channel III, i.e. interaction with the $^4\Pi$ state, is most important. The time evolution is clearly nonexponential and even the relative order of importance of the individual channels varies with time. The population of the initial vibrational level v = 5 decays even faster. For illustration purposes we also include an exponential function with a lifetime corresponding to that of $|\Psi_A(t)|^2$. Fig. 8(b) presents the time evolution of some neighbouring populations for initial preparation of ions in v = 5. Within the first 15 fs populations build up in the nearest neighbour levels v = 4 and v = 6. The maximum population in these levels

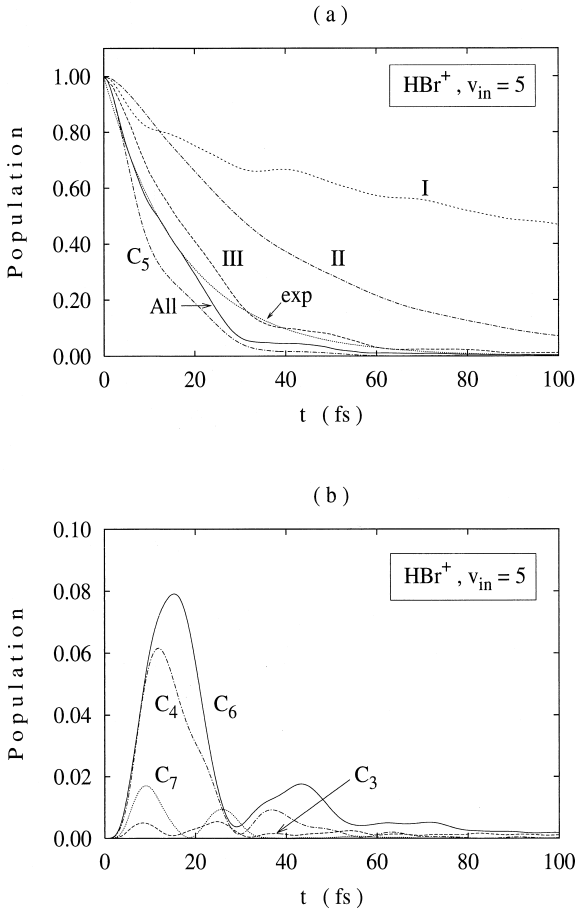

Fig. 8. Predissociation dynamics of HBr^+ ions from the initial level v = 5. (a) Time evolution of $|\Psi_A(t)|^2$ and the population $C_5(t)$, for comparison an exponential function (exp) is shown; $|\Psi_A(t)|^2$ obtained when taking into account only one of the three reaction channels (I, II, and III) separately are also shown. (b) Population of the neighbouring levels 3, 4, 6, and 7.

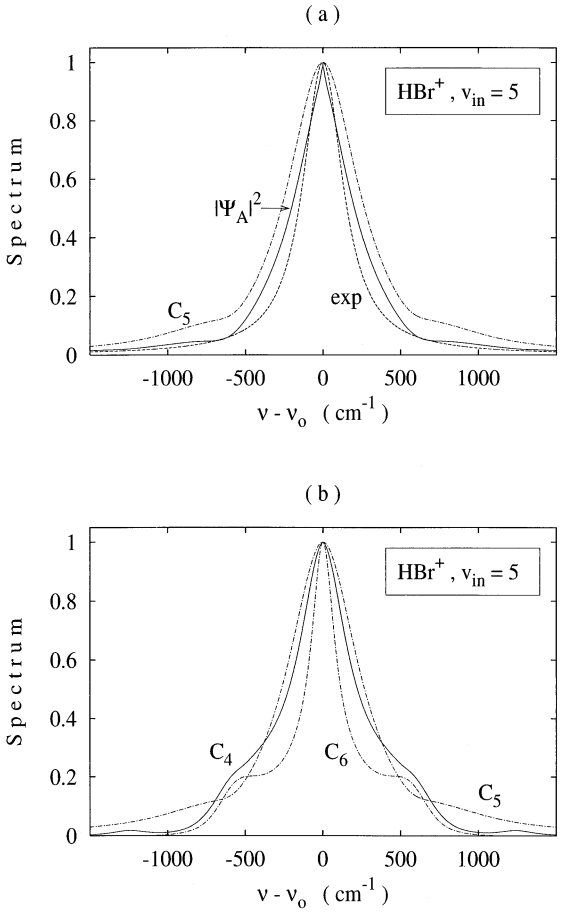

Fig. 9. Predissociation spectra of HBr^+ ions initially prepared in v = 5. (a) Predissociation spectrum of $|\Psi_A(t)|^2$ (solid line), and the population C_5 (dot-dashed line); for comparison a Lorentzian function with width 313.5 cm^{-1} (dashed line) is shown. (b) Predissociation spectra of the neighbouring populations C_4 and C_6 together with initial population C_5.

is about 0.08 and 0.06 referenced to the initial population at time zero [$C_5(t = 0) = 1$). However, this implies that at a given time, e.g. 18 fs, the population in the $v = 6$ state is only a factor of 4 smaller than that in the initially excited state (v = 5) at this time. The population in the second nearest levels v = 3 and v = 7 is even smaller, but still significant. All these populations show oscillations with a frequency of about 30 fs, however, these are strongly damped.

This temporal representation shall again be complemented by the corresponding spectral representation (see Fig. 9). Clearly neither the spectrum of the population C_5 [see Fig. 9(a)], nor that of $|\Psi_A(t)|^2$ are Lorentzian. Most interesting, the width of the spectrum of $|\Psi_A(t)|^2$ is significantly smaller than that of a Lorentzian near the top of the spectrum. The full width at half maximum, however, of C_5 and of $|\Psi_A(t)|^2$ is significantly larger than that of the Lorentzian function shown. The latter is the Fourier transform spectrum of the exponential shown in Fig. 8(a). In the temporal representation $|\Psi_A(t)|^2$ and this ex-

ponential function agreed quite well for short times but rather poorly for longer times. The agreement between the FFT spectrum of $|\Psi_A(t)|^2$ and the exponential, on the other hand, is good for the high frequency components, but poor for frequencies close to the center frequency. Of course this bears important implications for the analysis of experimental spectra recorded in the frequency domain. It implies that restoring predissociation dynamics from frequency domain spectra is difficult in the case of nonexponential decay. Fig. 9(b) shows the spectra of the populations of the neighbouring vibrational levels, v = 4 and 6. For comparison the spectrum of C_5 is shown again. In contrast to the latter C_4 and C_6 exhibit marked wings at frequencies of about ± 550 cm^{-1}. Similar to the situation discussed for HCl^+ in the initial vibrational level v = 11 (cf. Fig. 6) these positions correspond to the energies of the neighbouring vibrational levels (± 516 cm^{-1} for v = 6 and ± 536 cm^{-1} for v = 4). However, since the predissociation is extremely fast for HBr^+, v = 5 (17.1 fs), these sidebands are not fully resolved in the frequency domain. It is interesting to note, that even the position of the second nearest vibrational levels is observed in the spectrum of C_4 around ± 1200 cm^{-1}. For comparison: the unperturbed eigenenergies would appear at ± 1011.6 cm^{-1} (v = 7) and 1095.5 cm^{-1} (v = 3).

The initial vibrational level v = 5 is the one with the shortest lifetime for the predissociation of HBr^+ ions. For higher vibrational levels the lifetime increases to the order of about 100 fs. This is still significantly shorter than the lifetimes for the higher vibrational levels in the HCl^+. For HBr^+ ions initially prepared in the vibrational level v = 9 the predissociation dynamics is illustrated in Fig. 10. Fig. 10(a) displays the decay of $|\Psi_A(t)|^2$ taking into account all channels simultaneously (All) and each one of the channels separately (I, II, and III). Evidently channel number II (interaction with the $^2\Sigma^-$ state) is most important for long times. However, for the first 30 fs channel III is more important. Thus, we note that the three reaction channels do not work independently for this vibrational level. Competition between their contributions does indeed play a major role. This is further supported by comparing the sum of lifetimes

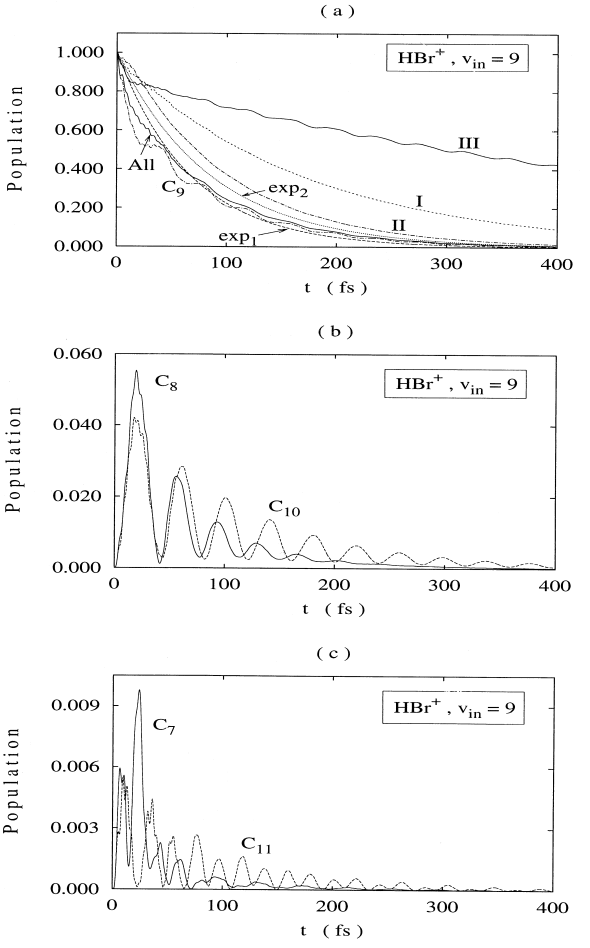

Fig. 10. Predissociation dynamics of HBr^+ ions from the initial level v = 9. (a) Time evolution of $|\Psi_A(t)|^2$ including all channels (all), and including only one particular channel (I, II, and III), and the population $C_9(t)$, for comparison two different exponential functions (exp_1 and exp_2) with lifetimes of 66.7 and 84.8 fs, respectively, are also shown. (b) Time evolution of the population of the nearest neighbour levels, C_8 and C_{10}. (c) Time evolution of the population of the second nearest neighbour levels, C_7 and C_{11}.

of the individual channels (88.9 fs) with that of $|\Psi_A(t)|^2$ taking into account all channels (66.7 fs). Fig. 10(a) also presents the time evolution of the initial population C_9. Here we notice almost step-like behavior up to about 100 fs, indicating extensive redistribution of population. For discussion of the spectral representation of these predissociation dynamics (see below) we also include two exponential functions in Fig. 10(a). One of these functions was

chosen to agree quite well with $|\Psi_A(t)|^2$ for short times and one for long times.

Fig. 10(b) and (c) show the population of the vibrational levels of nearest neighbours, C_8 and C_{10}, and second nearest neighbours, C_7 and C_{11}, respectively. Here the population of nearest neighbours exhibits extended oscillations over the entire time range shown (400 fs). This is possible because the predissociation lifetime for this initial level, v = 9, is long enough. We recall that for the initial level v = 5 [cf. Fig. 8(b)] the oscillation of population of nearest neighbours was basically damped to zero after 100 fs. Similar to the situation for the initial level v = 5, here the period of the oscillations is slightly shorter for the lower neighbour, C_8, compared to the upper neighbour, C_{10}. Both populations are built up in phase. They have an opposite phase at about 200 fs. But beyond this time oscillation has died for C_8. Again this reflects the shorter lifetime of the vibrational level 8 as compared to level 10. The maximum population of C_8 and C_{10} is about 10% of the population in the initial level at a given time. The population of second nearest neighbours [Fig. 10(c)] is almost an order of magnitude smaller. Since the lifetime of the vibrational level 11 is significantly longer than that of level 7, the oscillation of population extends to much longer time for the former.

The spectral representation of the populations C_8, C_9, and C_{10} is shown in Fig. 11. All populations exhibit a resonance at the central frequency ν_0. The width of this resonance is largest for C_8 and smallest for C_{10}, in line with the lifetimes discussed above. We note that side bands are observed at about ± 410 cm^{-1} for C_{10} and ± 430 cm^{-1} for C_8. The positions of the corresponding neighbouring vibrational levels are indicated by arrows. Sidebands are hardly discernible for the population of the initial level C_9.

Fig. 12 illustrates the spectrum of the population C_9 and of the wave packet in comparison with the spectra of the two exponential functions shown in Fig. 10(a). Most interestingly the spectrum of the $|\Psi_A(t)|^2$ and of C_9 appear to agree well with the spectrum of the second exponential (exp_2), but rather poor with that of the first exponential (exp_1). At first glance this is surprising, since the latter seems to agree much

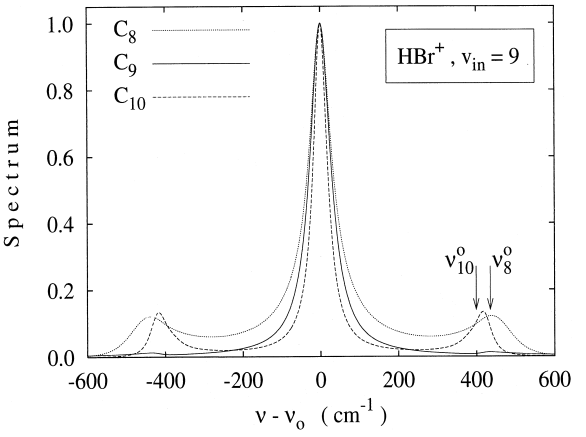

Fig. 11. Predissociation spectra of HBr^+ in the initial level $v = 9$. Populations of the vibrational levels 8, 9, and 10.

better with $|\Psi_A(t)|^2$ and C_9 in the temporal representation. However, this statement is only correct for the first 200 fs. Beyond this time the second exponential agrees much better with $|\Psi_A(t)|^2$ and C_9, and it is this time range which seems to be most relevant for the spectral representation. Again this bears important implications for the interpretation of experimental spectra. Let us assume one measures a spectrum similar to the symbols in Fig. 12. Further assuming exponential decay one would probably fit this spec-

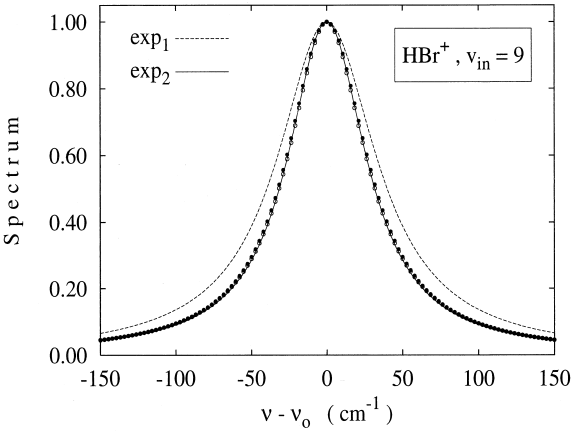

Fig. 12. Predissociation spectra of HBr^+ in the initial level v = 9. Comparison of the spectrum of $|\Psi_A(t)|^2$ (open circles), C_9 (closed circles) and of the two exponentials shown in Fig. 10(a) as indicated.

trum with a Lorentzian function similar to the solid line. However, in the temporal representation this would lead to a time evolution which does not give a good number for the $1/e$ decay time. This demonstrates that in the case of nonexponential decay it is very important to obtain spectra with high signal to noise ratio not only at the resonance center but also at the wings. We conclude that it will be rather difficult to analyze experimental frequency domain spectra in the case of nonexponential decay.

4. Summary and discussion

We have investigated the predissociation dynamics of HCl^+ and HBr^+ ions from a wide range of vibrational levels in the $^2\Sigma^+$ electronic state by numerical solution of coupled time-dependent Schrödinger equations based on ab initio potential energy data. For both systems the predissociation lifetime decreases in going from the threshold ($v = 7$ for HCl^+ and $v = 2$ for HBr^+) to the next higher vibrational states. The smallest lifetime is observed for $v = 8$ in the HCl^+ ion ($\tau = 160$ fs), and for $v = 5$ in the HBr^+ ion ($\tau = 17.1$ fs). For both molecular ions this occurs close to the crossing between the three repulsive electronic states and the predissociating $^2\Sigma^+$ electronic state. However, even the smallest lifetime in the HCl^+ is still larger than that of most vibrational levels in the HBr^+. This is due to the fact that the spin–orbit coupling, which facilitates this predissociation, is about a factor of 5 smaller in HCl^+ compared to HBr^+. In going to even higher vibrational levels the lifetime increases again.

For most of the vibrational levels in the HCl^+ the predissociation dynamics follows an exponential decay in the time domain. Only weak oscillations in the population of the vibrational states is observed. In contrast to this the predissociation dynamics is clearly nonexponential in the HBr^+ ion and pronounced oscillations are observed for the population of vibrational states. This indicates extensive redistribution of population between the initial and the neighbouring vibrational levels. Similar oscillations have, e.g. been observed in the predissociation of $HCo(CO)_4$ [29]. These oscillations are due to the propagation of the wave packet for electronic wave functions which are not eigenfunctions of the total system Hamiltonian, $H_{tot} = H_0 + H_{so}$. In principle one could obtain the eigenfunctions of the total Hamiltonian by diagonalization methods. The resulting wave function would then have dominant contributions from the basis function Ψ_A, but also smaller contributions from Ψ_I, Ψ_{II}, and Ψ_{III}. The latter contributions would be larger for the HBr^+ than for HCl^+ due to the larger spin–orbit coupling. However, we know of no easy way to prepare these "mixed" eigenstates experimentally.

Very often dynamic information is derived from experimental frequency domain spectra and the question has always been: to what extent is this approach valid? In general there is no problem as long as one deals with truly exponential decay and homogenous linewidth. Here the title systems of this work offer the possibility to compare a system with predominant exponential decay to one with predominantly nonexponential decay. Thus, for several initial vibrational states in the HCl^+ and HBr^+ the temporal representation of the predissociation dynamics has been complemented by the corresponding spectral representation obtained by FFT. For the HCl^+ the calculated spectra are very close to Lorentzian, which is not surprising in the light of the exponential character of the decay dynamics. For the HBr^+, however, pronounced deviations from Lorentzian line shapes are observed. This is a consequence of the nonexponential character of the decay dynamics in this system. For further analysis we have compared time evolution and the spectra of HBr^+ with model exponential decay functions and Lorentzian line shapes, respectively. Here, the most important result is, that Lorentzian functions which fit the central part of the spectrum (small $\nu - \nu_0$) well, lead to good agreement for the long-time behavior of the dynamics, whereas a good fit to the wings of the spectrum leads to reasonable short time behavior. The problem we want to point out is, that the signal to noise ratio of experimental frequency domain spectra is often poor in the wings. Thus, we conclude that the derivation of dynamic information from frequency spectra is diffi-

cult when the competition between different reaction channels leads to nonexponential decay. In the future we plan to apply the results of this work to the analysis of the state selective predissociation spectra of HCl^+ [16] and HBr^+ [7]. There we will also take into account the formation of molecular ions via the $A\ ^2\Sigma^+ \leftarrow X\ ^2\Pi_i$ transition. Ultimately this will hopefully enable us to compare calculated absorption spectra to the experimental predissociation spectra.

Acknowledgements

Support of this work by the Deutsche Forschungsgemeinschaft via project nos. We 1330/3 and SFB 450/C1 is gratefully acknowledged. It is a pleasure to thank Professor J. Manz for many stimulating discussions and for making the computer infrastructure of his group available to us.

References

[1] D.R. Yarkony, J. Phys. Chem. 100 (1996) 18612.
[2] P. Baltzer, M. Larsson, L. Karlsson, M. Lundqvist, B. Wannberg, Phys. Rev. A 49 (1993) 737.
[3] A. Yencha, A.J. Cormack, R.J. Donovan, K.P. Lawley, A. Hopkirk, G.C. King, Chem. Phys. 238 (1998) 133.
[4] F. Norling, Z. Phys. 95 (1935) 179.
[5] R.F. Barrow, A. Count, Proc. Phys. Soc., London, Sect. A 66 (1953) 617.
[6] M.J. Haugh, K.D. Bayes, J. Phys. Chem. 75 (1971) 1472.
[7] M. Penno, A. Holzwarth, K.-M. Weitzel, J. Phys. Chem. A 102 (1998) 1927.
[8] A. Banichevich, R. Klotz, S.D. Peyerimhoff, Mol. Phys. 75 (1992) 173.
[9] B.A. Heß, C.M. Marian, S.D. Peyerimhoff, in Modern Electronic Structure Theory, Part I, Advanced Series in Physical Chemistry, Vol. 4, D.R. Yarkony (Ed.), World Scientific, Singapore, 1995, p. 152.
[10] A. Mank, T. Nguyen, J.D.D. Martin, J.W. Hepburn, Phys. Rev. A 51 (1995) R1.
[11] D. Edvardsson, P. Baltzer, L. Karlsson, M. Lundqvist, B. Wannberg, J. Electron Spectrosc. Relat. Phenom. 73 (1995) 105.
[12] A.J. Yencha, A.G. McConkey, G. Dawber, L. Avaldi, M.A. MacDonald, G.C. King, R.I. Hall, J. Electron Spectrosc. Relat. Phenom. 73 (1995) 217.
[13] A. Yencha, A.J. Cormack, R.J. Donovan, A. Hopkirk, G.C. King, Chem. Phys. 238 (1998) 109.
[14] F. Norling, Z. Phys. 104 (1937) 177.
[15] W.D. Sheasley, C.W. Mathews, J. Mol. Spectrosc. 47 (1973) 420.
[16] M. Penno, A. Holzwarth, K.-M. Weitzel, Mol. Phys. 97 (1999) 43.
[17] S.D. Peyerimhoff, A. Banichevich, unpublished results.
[18] A.D. Pradhan, K.P. Kirby, A. Dalgarno, J. Chem. Phys. 95 (1991) 9009.
[19] G. Wentzel, Z. Phys. 43 (1927) 524; 29 (1927) 321.
[20] M.V. Korolkov, K.-M. Weitzel, Chem. Phys. 252 (2000) 209.
[21] M.V. Korolkov, G.K. Paramonov, Phys. Rev. A 57 (1998) 4998.
[22] C.C. Marston, G.G. Balint-Kurti, J. Chem. Phys. 91 (1989) 3571.
[23] S.G. Lias, J.E. Bartmess, J.F. Liebman, J.L. Holmes, R.D. Levin, W.G. Mallard, J. Phys. Chem. Ref. Data 17, Suppl. 1 (1988).
[24] R.J. Buenker, S.D. Peyerimhoff, W. Butscher, Mol. Phys. 35 (1978) 771.
[25] R. McWeeny, B.T. Sutcliffe, Methods of Molecular Quantum Mechanics, Academic, New York, 1969.
[26] M.D. Feit, J.A. Fleck, A. Steiger, J. Comput. Phys. 47 (1982) 412.
[27] R.N. Bisseling, R. Kosloff, J. Manz, J. Chem. Phys. 83 (1985) 993.
[28] G.G. Balint-Kurti, R.N. Dixon, C.C. Marston, A.J. Mulholland, Comput. Phys. Commun. 63 (1991) 126.
[29] C. Daniel, M.-C. Heitz, J. Manz, C. Ribbing, J. Chem. Phys. 102 (1995) 905.